PERFORMANCE ANALYSIS OF RIS-ASSISTED WIRELESS SYSTEMS WITH CHANNEL AGING AND SPATIAL CORRELATION

Yu Lu[1], Yan Zhang[1], Jiayi Zhang[1], Bo Ai[1]
[1]The School of Electronic and Information Engineering, Beijing Jiaotong University, Beijing, China

NOTE: Corresponding author: Jiayi Zhang, jiayizhang@bjtu.edu.cn

Abstract – *Reconfigurable Intelligent Surfaces (RISs) have caught wide attention for their advantages in dealing with the blocking obstacles in wireless communications. In this paper, we present a detailed analysis of RIS-assisted multiple-input single-output systems taking into account the joint effects of spatial correlation of the RIS elements and channel aging caused by users' relative movements. More specifically, a novel closed-form expression for the Spectrum Efficiency (SE) with maximum ratio transmission precoding is given. Monte Carlo simulation results verify the accuracy of the analytical results. It is proved that the channel aging phenomenon degrades the system performance while the application of a RIS can compensate for the loss, and the longer transmission time results in the more severe effect of channel aging on the system performance. Moreover, the spatial correlation of the RIS elements degrades communication quality and the SE. In addition, increasing the size of the RIS elements can improve the SE.*

Keywords – Channel aging, reconfigurable intelligent surface, spatial correlation, spectral efficiency

1. INTRODUCTION

Fifth Generation (5G) technologies are applied in high-frequency communication like massive Multiple-Input Multiple-Output (MIMO), small cells, and millimeter wave communication. One of the challenges is that the blocking of obstacles in the transmission environment seriously affects the quality of the transmitted signals [1][2]. To solve this problem, the use of a Reconfigurable Intelligent Surface (RIS) has caught wide attention. A RIS is a passive device composed of an array of intelligent reflecting elements, where each element can change the phase and amplitude of the imping signals independently [3][4][5][6]. The reflecting signals can be superimposed constructively with the signals from other links to enhance the strength of the desired signals and improve the system performance [7][8].

In the previous papers on RIS-assisted wireless communication systems, they mainly assumed Rayleigh, Rician, and Nakagami-*m* fading channels [9][10]. For instance, by assuming Rayleigh fading channels, the author in [11] studied the achievable rate of the cell-edge users in the RIS-assisted orthogonal frequency division systems. In [12], Maximum Mean Sum Error (MMSE) estimation of the RIS-assisted communication systems was carried out by using the ON/OFF protocol over Rayleigh fading channels, and the Signal to Interference Rate (SINR) and sum rate of the considered system are analyzed. Furthermore, in [13], the authors analyzed the normalized mean square error and SINR of the RIS-assisted Multiple-Input Multiple-Output (MISO) systems through MMSE estimation over the Rayleigh fading channels. In addition, by assuming Rician fading channels, Central Limit Theory (CLT) was employed in [14] to estimate RIS-assisted channels and studied the Outage Probability (OP) and Average Symbol Error Probability (ASEP) of the system. Moreover, in [15], the authors analyzed the OP, the ASEP, and the achievable rate of the RIS-assisted systems by assuming Nakagami-*m* fading channels.

However, existing research has not fully studied the time-varying channels. Most research ([11]-[15]) is based on a simple block fading model, that is, the channel characteristics in a coherent block are approximately constant. However, due to the relative movement between the users and the Base Station (BS)/RIS and the changes in the signal transmission environment, the performance of the actual channel changes continuously over time. These factors cause the so-called channel aging phenomenon. Channel aging will lead to the mismatch between the current channel and the estimated channel, which will degrade system performance [16][17]. In [17], the authors studied the effect of channel aging on the MIMO system. The normalized Doppler shift is used to represent the influence of channel aging on the system. The Doppler shift is the change in the frequency of received waves when an observer is moving relative to the source of the wave. If either the source or the observer is moving toward the other, the observer will perceive the sound at a higher frequency than that at which it was generated because the observer captures more waves per second. Alternatively, if the source and the observer are moving away from each other, the observer will perceive a lower frequency [18]. The simulation results show that the increase of normalized Doppler shift would decrease the sum rate of the system. In [19], the effect of channel aging on the cell-free MIMO system was analyzed, and the change of the system SE showed that the channel aging effect would reduce

Table 1 – Related work on analysis of RIS-assisted wireless system

Reference	RIS	Channel model	Channel estimation	Channel aging	Spatial correlation
[22]	✓	Rayleigh	MMSE, Deep Learning	×	×
[23]	✓	Rayleigh	MMSE	✓	×
[24]	✓	Rician	MMSE	×	✓
[25]	×	Rayleigh	LMMSE	×	×
[26]	×	Not mention	WMMSE	×	×
[27]	×	Rayleigh	LMMSE	×	×

the efficiency of the statistical channel cooperation power control. In [20], the authors studied the SINR of the receiver and analyzed the SE of the uplink and downlink, and derived the conclusion that increasing the number of transmitted antennas of the BS can alleviate the negative effect brought by the channel aging phenomenon.

Moreover, spatial correlation is one of the key characteristics of RIS. Most of the existing papers assume independent channels in the RIS-assisted systems, which is not accurate for performance analysis. In [21], the authors gave a new definition of channel hardening in RIS-assisted communications, and an accurate channel fading model was proposed by considering the spatial correlation of the RIS elements. The simulation results revealed that the system SNR variations in the case of random phases remain large since there is no hardening. Thus, the RIS-related channel should be properly configured to benefit from channel hardening and to improve system performance. In Table 1 we summarize the related work on different RIS-assisted wireless systems based on their channel model, method of channel estimation, etc.

To fill up these gaps, in this paper, considering the spatially correlated Rayleigh fading channels, we use the MMSE estimator to obtain the Channel State Information (CSI). The BS computes the estimates of the channel parameters based on the received pilot signal transmitted by the receiver and achieves the minimum mean square error between the true and estimated channel by exploiting prior knowledge of the channel's large-scale fading statistics based on the Bayesian estimation [28]. After that we derive the expressions of system Spectral Efficiency (SE) by adopting Maximum Ratio Transmission (MRT) precoding at the BS, and analyze the impact of different parameters on the SE. Monte Carlo results verify the correctness of the derived equations. The simulation results show that RIS can make up for the negative effect brought by channel aging, and the increase of signal transmission time increases the influence of channel aging on the system. Furthermore, considering the spatial correlation of RIS elements will decrease the SE of the system. In addition, increasing the size of RIS elements can improve system performance.

The remainder of this paper is organized as follows: In Section 2, we propose the system and channel models. In Section 3, the achievable sum SE for RIS-assisted systems is proposed. In Section 4, numerical results are presented to confirm the accuracy of the analytical results. In Section 5, we conclude the paper.

Notation: We use bold small letters $\boldsymbol{x}$ and bold capital letters $\boldsymbol{X}$ to represent column vectors and matrices, $[\boldsymbol{x}]_m$ represents the m-th entry of $\boldsymbol{x}$. $[\boldsymbol{X}]_{m,n}$ represents the entry in the m-th row and n-th column of $\boldsymbol{X}$. $\mathbb{C}^M$ represents complex M-dimensional vectors and $\mathbb{C}^{M\times N}$ represents complex M×N matrices. $(\cdot)^*$, $(\cdot)^{\mathrm{T}}$, $(\cdot)^{\mathrm{H}}$ and $(\cdot)^{-1}$ represent the conjugate, transpose, conjugate transpose, and inverse, respectively. $\mathrm{tr}(\cdot)$, $|\cdot|$, $\mathbb{E}(\cdot)$, $\mathrm{Var}(\cdot)$ and $\triangleq$ represent trace operator, absolute operator, expectation operator, variance operator and definition, respectively. $\otimes$ represents Kronecker product and $\|\cdot\|$ represents Euclidean norm of a vector. $\mathcal{CN}(0, \boldsymbol{R})$ represents a circularly symmetric complex Gaussian distribution with a zero mean vector and a covariance matrix $\boldsymbol{R} \succeq 0$.

2. SYSTEM MODELS

In the considered system, we assume that the BS employs multiple antennas to transmit the signal to each user to obtain the high gain of the received signal. We also assume that each user has the same characteristics except for their start position. Thus, a MISO system model shown in Fig 1 is considered. We assume that K single-antenna users simultaneously communicate with an N_{t}-antenna BS $(K < N_{\mathrm{t}})$. The RIS comprised of M reflecting elements and a controller is deployed to assist communication between the users and the BS. To achieve channel hardening and an improvement of system performance, the effect brought by the spatial correlation of RIS elements on the channel between the RIS and the user is consid-

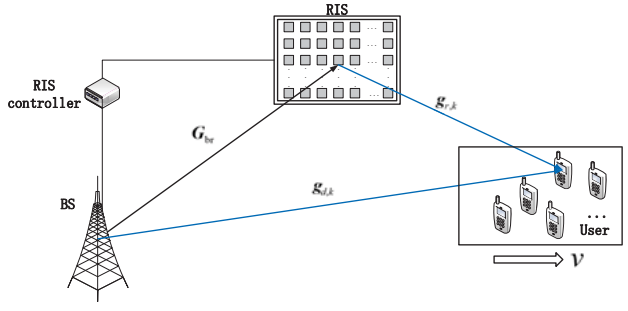

Fig. 1 – An RIS-assisted MISO system

ered [29]. The BS cannot only transmit signals directly to the user through the direct link, but also adjust the phase of RIS elements so that the signals can be reflected and transmitted to the user through the cascade link. Furthermore, we assume that the BS and the RIS remain static while the users move with the same velocity v [17]. The relative movement between the user and BS/RIS and the changes in the environment results in the channel aging phenomenon. We assume that the Line-of-Sight (LoS) link cannot be established between the BS and the RIS due to the spatial blockages between them, and the independent Rayleigh fading models are adopted because of the rich scatters between them [30][31]. The channel characteristics between BS/RIS and users change over time due to the relative movement of users [31]. We assume that channel coefficients remain constant within one symbol while changing across different symbols [32].

During the transmission of *n*-th symbol, the channel matrix of the direct link between the BS and users can be expressed as $\boldsymbol{G}_{\mathrm{d}}[n] = [\boldsymbol{g}_{\mathrm{d},1}[n], ..., \boldsymbol{g}_{\mathrm{d},k}[n], ..., \boldsymbol{g}_{\mathrm{d},K}[n]] \in \mathbb{C}^{N_t \times K}$, where $\boldsymbol{g}_{\mathrm{d},k}[n] \in \mathbb{C}^{N_t \times 1}$ represents the channel between the BS and user *k*. Specifically, $\boldsymbol{g}_{\mathrm{d},k}[n]$ can be expressed as

$$\boldsymbol{g}_{\mathrm{d},k}[n] = \sqrt{\beta_{\mathrm{d},k}}\boldsymbol{h}_{\mathrm{d},k}[n],\ \forall k \in \{1, ..., K\} \qquad (1)$$

where $\boldsymbol{h}_{\mathrm{d},k}[n] \in \mathbb{C}^{N_t \times 1}$ represents the small scaling fading coefficiency between user *k* and the BS, $\boldsymbol{h}_{\mathrm{d},k}[n] \sim \mathcal{CN}(0, \boldsymbol{I}_{\mathrm{N}_t})$, $\beta_{\mathrm{d},k}$ represents the path loss of direct link, which is assumed to be constant during the transmission of the signal. For the cascade links of BS-RIS-user *k*, based on the Rayleigh fading model, the channel between the BS and RIS can be denoted as $\boldsymbol{G}_{\mathrm{br}} = [\boldsymbol{g}_{\mathrm{br}1}, ..., \boldsymbol{g}_{\mathrm{br}m}, ..., \boldsymbol{g}_{\mathrm{br}M}] \in \mathbb{C}^{N_t \times M}$, where the *m*-th column vector $\boldsymbol{g}_{\mathrm{br}m} \in \mathbb{C}^{N_t \times 1}$ represents the channel coefficient between the BS and the *m*-th element of RIS. $\boldsymbol{G}_{\mathrm{br}}$ remains constant within a frame duration τ_c, but changes over different symbols. The channel between the RIS and user *k* can be denoted as $\boldsymbol{g}_{\mathrm{r},k}[n] = [g_{\mathrm{r},k1}[n], ..., g_{\mathrm{r},km}[n], ..., g_{\mathrm{r},kM}[n]]^{\mathrm{T}} \in \mathbb{C}^{M \times 1}$, where $g_{\mathrm{r},km}[n]$ represents the channel coefficient between user *k* and *m*-th element of the RIS. Thus, the cascaded channel can be represented by $\boldsymbol{G}_k[n] = \boldsymbol{G}_{\mathrm{br}}\boldsymbol{\Phi}[n]\boldsymbol{g}_{\mathrm{r},k}[n]$, where $\boldsymbol{\Phi}[n] = \mathrm{diag}\{\alpha \exp(j\theta_1[n]), ..., \alpha \exp(j\theta_M[n])\} \in \mathbb{C}^{M \times M}$ represents the reflecting matrix of RIS, $\alpha \in [0, 1]$ and $\theta_m[n] \in [0, 2\pi]$ represent the amplitude and phase change of reflected signal. Due to the sparsity and serious path loss of the mmWave channel, in this paper we only consider the signal reflected by the RIS for the first time and ignore those reflected by the RIS two or more times [33]. What's more, we assume that the amplitude of the reflected signal reaches to its maximum, that is, $\alpha = 1$. We express $\boldsymbol{G}_k[n]$ as $\boldsymbol{G}_k[n] = \boldsymbol{G}_{0,k}[n]\boldsymbol{v}[n]$, where $\boldsymbol{G}_{0,k}[n] = [\boldsymbol{g}_{0,k1}[n], ..., \boldsymbol{g}_{0,km}[n], ..., \boldsymbol{g}_{0,kM}[n]] \in \mathbb{C}^{N_t \times M}$ represents the channel matrix of the cascaded links, $\boldsymbol{v}[n] = [\alpha \exp(j\theta_1[n]), ..., \alpha \exp(j\theta_M[n])]^{\mathrm{T}} \in \mathbb{C}^{M \times 1}$ represents the reflecting matrix of the RIS. Additionally, $\boldsymbol{g}_{0,km}[n]$ can be written as $\boldsymbol{g}_{0,km}[n] = \boldsymbol{g}_{\mathrm{brm}}g_{\mathrm{r},km}[n]$.

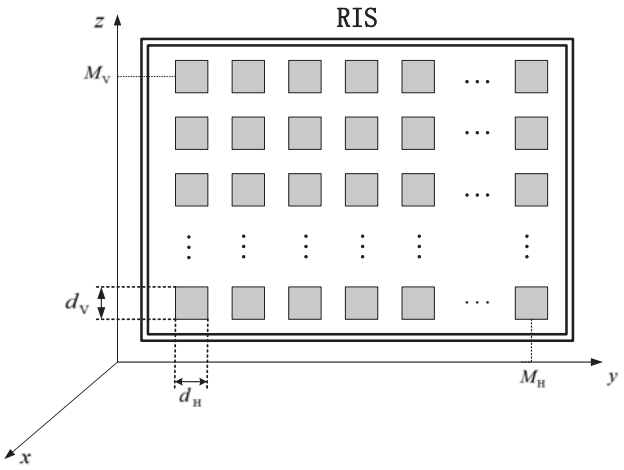

Fig. 2 – The 3D structure of the RIS with M_{H} columns and M_{V} rows

2.1 Spatial correlation of RIS elements

Fig. 2 presents the 3D structure of the RIS with M_{H} elements per column and M_{V} elements per row, $M = M_{\mathrm{H}}M_{\mathrm{V}}$ [34]. Each element has size $d_{\mathrm{H}} \times d_{\mathrm{V}}$, where d_{H} is the horizontal width and d_{V} is the vertical height. The area of each element is $A = d_{\mathrm{H}} \times d_{\mathrm{V}}$. We assume each element is closely arranged, so the total area of the RIS is MA. The location of the *n*-th (n ∈ {1,...,M}) element shown in Fig. 2 is

$$\boldsymbol{u}_n = [0, i(n)d_{\mathrm{H}}, j(n)d_{\mathrm{V}}]^{\mathrm{T}} \qquad (2)$$

where $i(n) = \mathrm{mod}\,(n-1, M_{\mathrm{H}})$ and $j(n) = \lfloor n - 1/M_{\mathrm{V}} \rfloor$ represent the horizontal and vertical indices of *n*-th element, respectively. Notice that $\mathrm{mod}\,(\cdot,\cdot)$ denotes modulus operation and $\lfloor \cdot \rfloor$ truncates the argument.

For any RIS deployed on a rectangular grid, the spatial correlation between RIS elements should be considered when $M_{\mathrm{H}} > 1$ and $M_{\mathrm{V}} > 1$. The channel model between the receiver and the RIS has been given in [21]

$$\boldsymbol{h} \sim \mathcal{CN}(\boldsymbol{0}, A\mu\boldsymbol{R}) \qquad (3)$$

$\boldsymbol{R}$ is the correlation matrix which can be expressed as

$$[\boldsymbol{R}]_{n,m} = \mathrm{sinc}(\frac{2\left\|\boldsymbol{u}_n - \boldsymbol{u}_m\right\|}{\lambda})\ n, m = 1, ..., N \qquad (4)$$

where $\mathrm{sinc}(x) = \sin(\pi x)/(\pi x)$.

Remark 1. For the expression of $\boldsymbol{R}$, since the sinc-function is only zero for non-zero integer arguments, all the elements must be separated by the integer times of $\lambda/2$ to achieve independent and identically distributed fading. However, this condition is not satisfied by the configuration of RIS, which proves the necessity of considering the spatial correlation between RIS elements.

2.2 Channel estimation

We now carry out the linear MMSE estimates of the direct and cascade links. We first obtain the estimates of the channel vectors at the initial state, then we can get the channel characteristic at other time instants based on temporal correlation between different time instants [35][36]. In the phase of transmitting pilot signals, we assume that the direct channel and cascade channel remain constant so that we can ignore the effect brought by channel aging [16]. *K* users transmit mutually orthogonal pilot sequences $\boldsymbol{\Psi} = [\boldsymbol{\psi}_1, ..., \boldsymbol{\psi}_K] \in \mathbb{C}^{\tau_p \times K}$ which satisfies $\boldsymbol{\Psi}^{\mathrm{H}} \boldsymbol{\Psi} = \boldsymbol{I}_K$, where $\boldsymbol{\psi}_k \in \mathbb{C}^{\tau_p \times 1}$ represents the pilot signals from user *k*. The pilot signals from different users satisfy $\boldsymbol{\psi}_i^{\mathrm{H}} \boldsymbol{\psi}_j = 0,\ \forall i \neq j$. For the direct link between the BS and user *k*, the received signal at BS can be presented as

$$\boldsymbol{Y}_{p\mathrm{d}}[0] = \sqrt{P_p}\boldsymbol{G}_{\mathrm{d}}[0]\boldsymbol{\Psi}^{\mathrm{H}} + \boldsymbol{Z}_{\mathrm{pd}}[0] \tag{5}$$

where $P_p = \tau_p P_u$ represents the power of the pilot signal, P_u is the average transmitting power of each user. $\boldsymbol{Z}_{\mathrm{pd}}[0] \in \mathbb{C}^{N_t \times \tau_p}$ is the received noise of BS at initial state, and $\boldsymbol{Z}_{p\mathrm{d}}[0] \sim \mathcal{CN}\left(\boldsymbol{0}, \sigma_b^2 \boldsymbol{I}_{N_{\mathrm{t}}}\right)$, where σ_b^2 is the variance of noise. Correlating the received signal with $1/\sqrt{P_p}\boldsymbol{\psi}_k$, we have

$$\tilde{\boldsymbol{y}}_{p\mathrm{d},k}[0] = \boldsymbol{g}_{\mathrm{d},k}[0] + \frac{1}{\sqrt{P_p}}\tilde{\boldsymbol{z}}_{\mathrm{pd}}[0] \tag{6}$$

where $\tilde{\boldsymbol{z}}_{pd}[0] = \boldsymbol{Z}_{p\mathrm{d}}[0]\boldsymbol{\psi}_k \sim \mathcal{CN}\left(0, \sigma_b^2 \boldsymbol{I}_{N_{\mathrm{t}}}\right)$. The optimum of $\boldsymbol{g}_{\mathrm{d},k}[0]$ that minimizes the mean squared error $\mathbb{E}[\|\boldsymbol{g}_{\mathrm{d},k}[0] - \hat{\boldsymbol{g}}_{\mathrm{d},k}[0]\|^2]$ is the MMSE estimate [22] . So that the MMSE estimation of $\boldsymbol{g}_{\mathrm{d},k}[0]$ can be expressed as [12]

$$\hat{\boldsymbol{g}}_{\mathrm{d},k}[0] = \left(1 + \frac{\sigma_b^2}{P_p \beta_{\mathrm{d},k}}\right)^{-1} \tilde{\boldsymbol{y}}_{p\mathrm{d},k}[0] \tag{7}$$

Therefore, $\boldsymbol{g}_{\mathrm{d},k}[0]$ can be written as

$$\boldsymbol{g}_{\mathrm{d},k}[0] = \hat{\boldsymbol{g}}_{\mathrm{d},k}[0] + \tilde{\boldsymbol{g}}_{\mathrm{d},k}[0] \tag{8}$$

where $\hat{\boldsymbol{g}}_{\mathrm{d},k}[0] \sim \mathcal{CN}\left(\boldsymbol{0}, \frac{P_p \beta_{\mathrm{d},k}^2}{\sigma_b^2 + P_p \beta_{\mathrm{d},k}} \boldsymbol{I}_{N_{\mathrm{t}}}\right)$. $\tilde{\boldsymbol{g}}_{\mathrm{d},k}[0] \sim \mathcal{CN}\left(\boldsymbol{0}, \frac{\beta_{\mathrm{d},k}\sigma_b^2}{\sigma_b^2 + P_p \beta_{\mathrm{d},k}} \boldsymbol{I}_{N_{\mathrm{t}}}\right)$ is the estimation error which is uncorrelated with $\hat{\boldsymbol{g}}_{d,k}[0]$. When we consider the direct channel and cascade channel simultaneously, the received signal at the BS can be expressed as

$$\boldsymbol{Y}_{pc}[0] = \sqrt{P_p}(\boldsymbol{G}_{\mathrm{d}}[0] + \boldsymbol{G}_{0\mathrm{c}}[0])\boldsymbol{\Psi}^{\mathrm{H}} + \boldsymbol{Z}_{pc}[0] \tag{9}$$

where $\boldsymbol{G}_{0c}[0] = [\boldsymbol{g}_{0,1}[0], ..., \boldsymbol{g}_{0,k}[0], ..., \boldsymbol{g}_{0,K}[0]] \in \mathbb{C}^{N_t \times K}$. Correlating the received signal with $1/\sqrt{P_p}\boldsymbol{\psi}_k$, we have

$$\boldsymbol{y}_{\mathrm{pc},k}[0] = \boldsymbol{g}_{\mathrm{d},k}[0] + \boldsymbol{g}_{0,k}[0] + \frac{1}{\sqrt{P_p}}\tilde{\boldsymbol{z}}_{\mathrm{pc}}[0] \tag{10}$$

where $\tilde{\boldsymbol{z}}_{\mathrm{pc}}[0] = \boldsymbol{Z}_{\mathrm{pc}}[0]\boldsymbol{\psi}_k$, and $\tilde{\boldsymbol{z}}_{\mathrm{pc}}[0] \sim \mathcal{CN}\left(\boldsymbol{0}, \sigma_c^2 \boldsymbol{I}_{N_{\mathrm{t}}}\right)$, where σ_c^2 is the power of received noise. From *(6)*, ignoring the channel estimation error in the receiving signal, the received signal at the BS can be obtained as

$$\tilde{\boldsymbol{y}}_{\mathrm{pc},k}[0] = \tilde{\boldsymbol{g}}_{\mathrm{d},k}[0] + \boldsymbol{g}_{0,k}[0] + \frac{1}{\sqrt{P_p}}\tilde{\boldsymbol{z}}_{\mathrm{pc}}[0] \tag{11}$$

From *(3)*, the channel between the BS and the RIS satisfies $\boldsymbol{g}_{\mathrm{r,k}} \sim \mathcal{CN}(\boldsymbol{0}, A\mu_1 \boldsymbol{R})$, the channel between the RIS and user *k* satisfies $\boldsymbol{g}_{\mathrm{r},km}[n] \sim \mathcal{CN}(\boldsymbol{0}, A\mu_2 \boldsymbol{R})$, where μ_1 and μ_2 denotes the path loss of the correspoding channel, respectively. We denote $\beta_{0,k}$ as the total path loss of the cascade links, so that we can get the MMSE estimation of $\boldsymbol{g}_{0,k}[0]$ as [12]

$$\hat{\boldsymbol{g}}_{0,k}[0] = \beta_{0,k}\left(\frac{\sigma_b^2 \beta_{\mathrm{d},k}}{\sigma_b^2 + P_p \beta_{\mathrm{d},k}} + \beta_{0,k} + \frac{\sigma_c^2}{P_p}\right)^{-1} \tilde{\boldsymbol{y}}_{\mathrm{pc},k}[0] \tag{12}$$

Thus $\boldsymbol{g}_{0,k}[0]$ can be written as

$$\boldsymbol{g}_{0,k}[0] = \tilde{\boldsymbol{g}}_{0,k}[0] + \hat{\boldsymbol{g}}_{0,k}[0] \tag{13}$$

where $\hat{\boldsymbol{g}}_{0,k}[0] \sim \mathcal{CN}\left(\boldsymbol{0}, \frac{\beta_{0,k}\hat{\sigma}_{e1,k}^2}{\hat{\sigma}_{e1,k}^2 + \hat{\sigma}_{e2,k}^2 + \hat{\sigma}_c^2 \hat{\sigma}_b^2} \boldsymbol{I}_{N_{\mathrm{t}}}\right)$, $\tilde{\boldsymbol{g}}_{0,k}[0]$ denotes the estimation error of cascade channel, $\tilde{\boldsymbol{g}}_{0,k}[0] \sim \mathcal{CN}\left(\boldsymbol{0}, \frac{\beta_{0,k}\sigma_{e2,k}^2 + \beta_{0,k}\sigma_c^2\sigma_b^2}{\sigma_{e2,k}^2 + \sigma_{e1,k}^2 + \sigma_c^2\sigma_b^2} \boldsymbol{I}_{N_{\mathrm{t}}}\right)$, where $\sigma_{e1,k}^2 \triangleq P_p \beta_{0,k}\left(\sigma_b^2 + P_p \beta_{\mathrm{d},k}\right)$, $\sigma_{e2,k}^2 \triangleq P_p \beta_{\mathrm{d},k}\left(\sigma_b^2 + \sigma_c^2\right)$.

2.3 Channel aging

Due to the relative movement between users and BS/RIS and the changes in the transmission environment, the transmission channel changes over different time instants, which leads to a so-called channel aging phenomenon. We assume that all the users move at the same velocity v. Fig. 3 shows the change of channel due to the channel aging effect. According to [32][37], $\boldsymbol{g}_{\mathrm{d},k}[n]$ and $g_{\mathrm{r},km}[n]$ can be represented by their initial states $\boldsymbol{g}_{\mathrm{d},k}[0]$ and $g_{r,km}[0]$, respectively

$$\boldsymbol{g}_{\mathrm{d},k}[n] = \rho_0[n]\boldsymbol{g}_{\mathrm{d},k}[0] + \bar{\rho}_0[n]\boldsymbol{e}_{\mathrm{d},k}[n] \tag{14}$$

$$g_{\mathrm{r},km}[n] = \rho_1[n]g_{\mathrm{r},km}[0] + \bar{\rho}_1[n]e_{\mathrm{r},km}[n] \tag{15}$$

According to the Jakes' model [38], $\rho_i[n]\ (i \in \{0,1\})$ denotes the relative parameter of channel at initial state and time *n* [16], $\rho_i[n] = J_0(2\pi n f_D T_s)$, where $J_0(\cdot)$ is the zeroth-order Bessel function of the first kind, $f_D = f_c v/c$ represents the maximum Doppler shift, f_c is the frequency of carrier, v is the moving velocity, c denotes the speed of light, T_s denotes the sampling interval. We assume that $\rho_i[n]\ (i \in \{0,1\})$ is known at the BS. Furthermore, $\bar{\rho}_i[n] = \sqrt{1 - \rho_i^2[n]}\ (i \in \{0,1\})$, $\boldsymbol{e}_{\mathrm{d},k}[n]$ and $e_{\mathrm{r},km}[n]$ represents the part of the current channel which

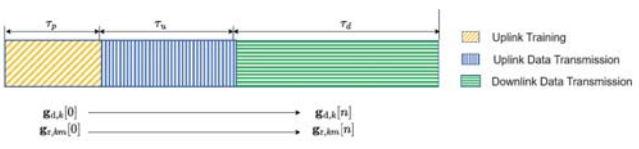

Fig. 3 – Illustration of the channel aging effect

is uncorrelated with the channel of initial time, which satisfy the condition that $[\boldsymbol{e}_{d,k}[n]]_{n_t} \sim \mathcal{CN}(0, \beta_{d,k})$ $(n_t = 1, ..., N_t)$ and $e_{\mathrm{r},km} \sim \mathcal{CN}(0,1)$, respectively.

Thus, $\boldsymbol{g}_{0,km}[n]$ can be written as

$$\begin{aligned}\boldsymbol{g}_{0,km}[n] &= \boldsymbol{g}_{\mathrm{brm}}(\rho_1[n] g_{\mathrm{r},km}[0] + \bar{\rho}_1[n] e_{\mathrm{r},km}) \\ &= \rho_1[n]\boldsymbol{g}_{\mathrm{brm}} g_{\mathrm{r},km}[0] + \bar{\rho}_1[n]\boldsymbol{g}_{\mathrm{brm}} e_{\mathrm{r},km}\end{aligned} \quad (16)$$

Define $\boldsymbol{e}_{0,km}[n] \triangleq \boldsymbol{g}_{\mathrm{brm}} e_{\mathrm{r},km}$, we can get $\boldsymbol{e}_{0,km}[n] \sim \mathcal{CN}\left(0, \beta_{0,k}\boldsymbol{I}_{N_\mathrm{t}}\right)$, thus, $\boldsymbol{g}_{0,km}[n]$ can be written as

$$\boldsymbol{g}_{0,km}[n] = \rho_1[n]\boldsymbol{g}_{0,km}[0] + \bar{\rho}_1[n]\boldsymbol{e}_{0,km}[n] \quad (17)$$

Then, the channel coefficient of the direct link considering the combined effect of channel estimation error and channel aging can be represented as

$$\begin{aligned}\boldsymbol{g}_{\mathrm{d},k}[n] &= \rho_0[n]\left(\hat{\boldsymbol{g}}_{\mathrm{d},k}[0] + \tilde{\boldsymbol{g}}_{\mathrm{d},k}[0]\right) + \bar{\rho}_0[n]\boldsymbol{e}_{\mathrm{d},k}[n] \\ &= \rho_0[n]\hat{\boldsymbol{g}}_{\mathrm{d},k}[0] + \tilde{\boldsymbol{e}}_{\mathrm{d},k}[n]\end{aligned} \quad (18)$$

where $\tilde{\boldsymbol{e}}_{\mathrm{d},k}[n] \triangleq \rho_0[n]\tilde{\boldsymbol{g}}_{\mathrm{d},k}[0] + \bar{\rho}_0[n]\boldsymbol{e}_{\mathrm{d},k}[n]$, and $\tilde{\boldsymbol{e}}_{\mathrm{d},k}[n] \sim \mathcal{CN}\left(\boldsymbol{0}, \left(\beta_{\mathrm{d},k} - \frac{(\rho_0[n])^2 P_p \beta_{\mathrm{d},k}^2}{\sigma_b^2 + P_p\beta_{\mathrm{d},k}}\right)\boldsymbol{I}_{N_\mathrm{t}}\right)$.

Similarly, the channel model of the cascade link can be represented as

$$\begin{aligned}\boldsymbol{g}_{0,km} &= \rho_1[n]\left(\hat{\boldsymbol{g}}_{0,km}[0] + \tilde{\boldsymbol{g}}_{0,km}[0]\right) + \bar{\rho}_1[n]\boldsymbol{e}_{0,km}[n] \\ &= \rho_1[n]\hat{\boldsymbol{g}}_{0,km}[0] + \tilde{\boldsymbol{e}}_{0,km}[n]\end{aligned} \quad (19)$$

where $\tilde{\boldsymbol{e}}_{0,km}[n] \triangleq \rho_1[n]\tilde{\boldsymbol{g}}_{0,km}[0] + \bar{\rho}_1[n]\boldsymbol{e}_{0,km}[n]$, and $\tilde{\boldsymbol{e}}_{0,km}[n] \sim \mathcal{CN}\left(\boldsymbol{0}, \left(\beta_{0,k} - \frac{\rho_1^2[n]\beta_{0,k}\sigma_{e1,k}^2}{\sigma_{e1,k}^2 + \sigma_{e2,k}^2 + \sigma_c^2\sigma_b^2}\right)\boldsymbol{I}_{N_\mathrm{t}}\right)$.

Remark 2. For equations *(18)* and *(19)*, the greater of the velocity v of the relative movement of the user, increase the value of the maximum Doppler shift f_D and decrease the value of $\rho_i[n]$ will increase the variance of $\tilde{\boldsymbol{e}}_{\mathrm{d},k}[n]$ and $\tilde{\boldsymbol{e}}_{0,km}[n]$, which will enlarge the difference between the channel characteristics of different times.

3. PERFORMANCE ANALYSIS

We investigate channel aging on system performance in the downlink transmission. Based on the channel reciprocity [17], the downlink channel matrix can be represented as the conjugate transpose of the uplink channel. Thus, in the phase of downlink signal transmission, the received signal at user *k* can be written as

$$y_k[n] = \left(\boldsymbol{g}_{\mathrm{d},k}^{\mathrm{H}}[n] + \boldsymbol{v}^{\mathrm{H}}[n]\boldsymbol{G}_{0,k}^{\mathrm{H}}[n]\right)\boldsymbol{x}[n] + \omega_k[n] \quad (20)$$

where $\boldsymbol{x}[n] = \boldsymbol{F}[n]\boldsymbol{s}[n]$ denotes the signal transmitted from the BS, and $\mathbb{E}[\|\boldsymbol{x}[n]\|^2] = \mathrm{Tr}(\boldsymbol{F}^{\mathrm{H}}[n]\boldsymbol{F}[n]) \le P_\mathrm{T}$, where P_T is the total power of the transmitted signal. $\boldsymbol{F}[n] = [\boldsymbol{f}_1[n], ..., \boldsymbol{f}_K[n]] \in \mathbb{C}^{N_\mathrm{t}\times K}$ represents the precoding matrix, $\boldsymbol{s}[n] = [s_1[n], ..., s_K[n]]^{\mathrm{T}} \in \mathbb{C}^{K\times 1}$ denotes received signal vector at users, which satisfies $\mathbb{E}(\boldsymbol{s}[n]) = 0$ and $\mathbb{E}(\boldsymbol{s}[n]\boldsymbol{s}^{\mathrm{H}}[n]) = \boldsymbol{I}_K$. $\omega_k[n]$ denotes the Additive White Gaussian Noise (AWGN) at user *k*, $\omega_k[n] \sim \mathcal{CN}(0, \sigma_k^2)$. Define $\boldsymbol{G}_k[n] \triangleq \boldsymbol{g}_{\mathrm{d},k}^{\mathrm{H}} + \boldsymbol{v}^{\mathrm{H}}[n]\boldsymbol{G}_{0,k}^{\mathrm{H}}[n]$, we have

$$\begin{aligned}\boldsymbol{G}_k[n] &= (\rho_0[n]\hat{\boldsymbol{g}}_{\mathrm{d},k}^{\mathrm{H}}[0] + \tilde{\boldsymbol{e}}_{\mathrm{d},k}^{\mathrm{H}}[n]) \\ &\quad + \boldsymbol{v}^{\mathrm{H}}[n](\rho_1[n]\hat{\boldsymbol{G}}^{\mathrm{H}}[0] + \tilde{\boldsymbol{E}}_{0,k}^{\mathrm{H}}[n]) \\ &= \bar{\boldsymbol{G}}_k[n] + \boldsymbol{G}_{\mathrm{e},k}[n]\end{aligned} \quad (21)$$

Where $\bar{\boldsymbol{G}}_k[n] \triangleq \rho_0[n]\hat{\boldsymbol{g}}_{\mathrm{d},k}^{\mathrm{H}}[0] + \rho_1[n]\boldsymbol{v}^{\mathrm{H}}[n]\hat{\boldsymbol{G}}_{0,k}^{\mathrm{H}}[0]$, $\boldsymbol{G}_{\mathrm{e},k} \triangleq \tilde{\boldsymbol{e}}_{\mathrm{d},k}^{\mathrm{H}}[n] + \boldsymbol{v}^{\mathrm{H}}[n]\tilde{\boldsymbol{E}}_{0,k}^{\mathrm{H}}[n]$, $\hat{\boldsymbol{G}}_{0,k}[0] = [\hat{\boldsymbol{g}}_{0,k1}[0], ..., \hat{\boldsymbol{g}}_{0,km}[0], ..., \hat{\boldsymbol{g}}_{0,kM}[0]]$ and $\tilde{\boldsymbol{E}}_{0,k}[n] = [\tilde{\boldsymbol{e}}_{0,k1}[n], ..., \tilde{\boldsymbol{e}}_{0,km}[n], ..., \tilde{\boldsymbol{e}}_{0,kM}[n]]$. Thus, the received signal at user *k* can be expressed as

$$\begin{aligned}y_k[n] &= \mathbb{E}\left(\boldsymbol{G}_k[n]\boldsymbol{f}_k[n]\right)s_k[n] + \sum_{j=1,j\neq k}^{K}\boldsymbol{G}_k[n]\boldsymbol{f}_\mathrm{j}[n]s_j[n] \\ &\quad + \boldsymbol{G}_k[n]\boldsymbol{f}_k[n]s_k[n] - \mathbb{E}\left(\boldsymbol{G}_k[n]\boldsymbol{f}_k[n]\right)s_k[n] + \omega_k[n]\end{aligned} \quad (22)$$

We use MRT precoding at the BS. The CSI known at the BS at time *n* is $\bar{\boldsymbol{G}}[n]$, the precoding matrix can be expressed as [12]

$$\boldsymbol{F}[n] = \zeta[n]\left(\bar{\boldsymbol{G}}[n]\right)^{\mathrm{H}} \quad (23)$$

where $\zeta^2[n] \triangleq 1/\,\mathrm{tr}\left(\bar{\boldsymbol{G}}[n]\left(\bar{\boldsymbol{G}}[n]\right)^{\mathrm{H}}\right)$ denotes the normalized coefficient of the precoding matrix. According to the use-and-then-forget capacity bound [39], the achievable SE of user *k* is lower bounded by

$$R_k = \frac{1}{\tau_c}\sum_{n=1}^{\tau_c-\tau_p}\log_2(1+\gamma_k[n]) \quad (24)$$

where $\gamma_k[n]$ is the SINR of user *k* at time *n*

$$\gamma_k[n] = \frac{\underbrace{\left|\mathbb{E}\left(\boldsymbol{G}_k[n]\boldsymbol{f}_k[n]\right)\right|^2}_{I_{0,kn}}}{\underbrace{\mathrm{Var}\left(\boldsymbol{G}_k[n]\boldsymbol{f}_k[n]\right)}_{I_{1,kn}} + \underbrace{\sum_{j=1,j\neq k}^{K}\mathbb{E}\left(\left|\boldsymbol{G}_k[n]\boldsymbol{f}_j[n]\right|^2\right)}_{I_{2,kn}} + \underbrace{\mathbb{E}\left(|\omega_k[n]|^2\right)}_{I_{3,kn}}} \quad (25)$$

The sum SE can be expressed as

$$R = \sum_{k=1}^{K}R_k \quad (26)$$

Corollary 1. The SINR of user *k* can be written as

$$\gamma_k[n] = \frac{I_{0,kn}}{I_{1,kn} + I_{2,kn} + I_{3,kn}} \quad (27)$$

where

$$I_{0,kn} = \zeta^2[n]\left(N_\mathrm{t}\left(\frac{\rho_0^2[n]p_p\beta_{d,k}^2}{\sigma_b^2 + P_p\beta_{\mathrm{d},k}} + \frac{M\rho_1^2[n]\beta_{0,k}\sigma_{e1,k}^2}{\sigma_{e1,k}^2 + \sigma_{e2,k}^2 + \sigma_b^2\sigma_c^2}\right)\right)^2 \quad (28)$$

$$I_{1,kn} = \left(\left(\beta_{\mathrm{d},k} - \frac{\rho_0^2[n] P_p \beta_{d,k}^2}{\sigma_b^2 + P_p \beta_{d,k}} \right) + M \left(\beta_{0,k} - \frac{\rho_1^2[n] \beta_{0,k} \sigma_{e1,k}^2}{\sigma_{e1,k}^2 + \sigma_{e2,k}^2 + \sigma_c^2 \sigma_b^2} \right) \right) \times \zeta^2[n] N_{\mathrm{t}} \left(\frac{\rho_0^2[n] P_p \beta_{d,k}^2}{\sigma_b^2 + P_p \beta_{d,k}} + \frac{M \rho_1^2[n] \beta_{0,k} \sigma_{e1,k}^2}{\sigma_{e1,k}^2 + \sigma_{e2,k}^2 + \sigma_c^2 \sigma_b^2} \right) \quad (29)$$

$$I_{2,kn} = \left(\left(\beta_{\mathrm{d},k} - \frac{\rho_0^2[n] P_p \beta_{\mathrm{d},k}^2}{\sigma_b^2 + P_p \beta_{d,k}} \right) + M \left(\beta_{0,k} - \frac{\rho_1^2[n] \beta_{0,k} \sigma_{e1,k}^2}{\sigma_{e1,k}^2 + \sigma_{e2,k}^2 + \sigma_c^2 \sigma_b^2} \right) \right) \times \sum_{j=1, j \neq k}^{K} \zeta^2[n] N_{\mathrm{t}} \left(\frac{\rho_0^2[n] p_p \beta_{\mathrm{d},j}^2}{\sigma_b^2 + p_p \beta_{\mathrm{d},j}} + \frac{M \rho_1^2[n] \beta_{0,k} \sigma_{e1,j}^2}{\sigma_{e1,j}^2 + \sigma_{e2,j}^2 + \sigma_c^2 \sigma_b^2} \right) \quad (30)$$

$$I_{3,kn} = \sigma_k^2 \quad (31)$$

Proof: See the appendix.

Remark 3. We can see from *(27)-(31)* that, with the increase of transmission power of pilot signal P_p and the number of BS antennas N_{t}, the desired signal power $I_{0,kn}$ increases while signal interference $I_{1,kn}$ and $I_{2,kn}$ decrease, which indicates that the increase of the above parameters can improve the SE of the system.

Remark 4. As for the number of the RIS elements *M*, when *M = 0*, *(25)* represents the SINR of a traditional MISO system without the assistance of the RIS. When the RIS has a large number of elements, that is, *M* approximates to infinity, the numerator and denominator increase simultaneously, thus *(25)* is approximated to be a constant.

4. NUMERICAL RESULTS

In this section, we verify the correctness of the equations by comparing the Monte Carlo results with analytical results. At the same time, we compare and analyze the impact of the number of reflecting elements *M*, transmit power of pilot signals P_p, temporal correlation coefficient $\rho_i[n]$ $(i \in \{0, 1\})$ and spatial correlation of RIS elements on SE.

The path loss of the direct channel $\beta_{d,k}$ can be expressed as $\beta_{d,k}[\mathrm{dB}] = \beta_0 - 10\xi \log_{10} d_{\mathrm{bu},k}$, where $\beta_0 = -40$ dB is the reference path loss, $\xi = 4.2$ is the path loss exponent, and $d_{\mathrm{bu},k}$ is the distance from the BS to user *k*. As for the cascaded channel, the path loss can be expressed as $\beta_{0,k} = G_{\mathrm{t}} G_{\mathrm{r}} d_{\mathrm{H}}^2 d_{\mathrm{V}}^2 \cos\theta_{\mathrm{t}} \cos\theta_{\mathrm{r}} / (16\pi^2 d_{\mathrm{br}}^2 d_{\mathrm{ru},k}^2)$, where G_{t} and G_{r} denote the transmit antenna gain and receive antenna gain, respectively. d_{H} and d_{V} represent the size of each RIS element. θ_t and θ_r represent the angle of elevation between the center of RIS and BS antenna and the antenna of user *k*, respectively. d_{br} and $d_{\mathrm{ru},k}$ represent the distance between the BS and the center of the RIS and the distance between the center of the RIS and user *k*, respectively [40]. We set $G_{\mathrm{t}} = 20$ dB, $G_r = 0$ dB, $d_{\mathrm{H}} = d_{\mathrm{V}} = \lambda/2$. λ denotes the wavelength of the signal, the carrier frequency is 2 GHz, the channel noise $\sigma_k^2 = -96$ dBm. Furthermore, we use the (x, y, z) coordinates (in meters) to describe the relative location of the BS, the RIS, and the users. BS is located at (-60, 0 ,10), the center of the RIS is located at (-50, 0, 6), and the users are in relative motion, and their positions are (60,0,10), (60.5,0,10), (61,0,10) and (61.5,0,10).

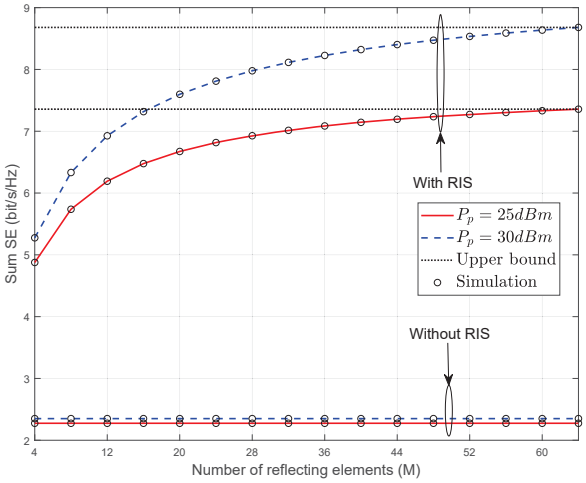

Fig. 4 – Sum SE versus *M* and P_p ($N_{\mathrm{t}} = 8$, $f_D T_s = 0.002$)

Fig. 4 shows the SE of RIS-assisted MISO systems under the condition of the different number of RIS elements *M* and the transmit power of pilot signal P_p. We can observe that the simulated results closely match with the analytical results, which validates the accuracy of the equations we derived. Moreover, compared with the traditional wireless communication systems, the application of the RIS can greatly improve the sum SE. The increase of the RIS elements can improve system performance, however, when the number of the elements reaches infinity, the sum SE becomes constant, which confirms the analysis in Remark 4. Moreover, the higher the transmit power, the stronger of the anti-interference ability of the transmitted signal and the higher the sum SE of the system. For example, when the number of RIS elements is 64, that is, $M = 64$, when we increase the transmit power of pilot signal from 25 dBm to 30 dBm, the SE increases by 18%.

Then, we use normalized Doppler shift $f_D T_s$ to represent the impact of channel aging on system performance. From *(14)* and *(15)*, the larger the value of $f_D T_s$, i.e., the faster the users move, the more seriously the impact of the channel aging on the system. Furthermore, Fig. 5 shows the relationship between users' average SE and transmission time under different $f_D T_s$ and the number of RIS elements. We can observe that the average SE decreases with time increases because of the channel aging effect, and

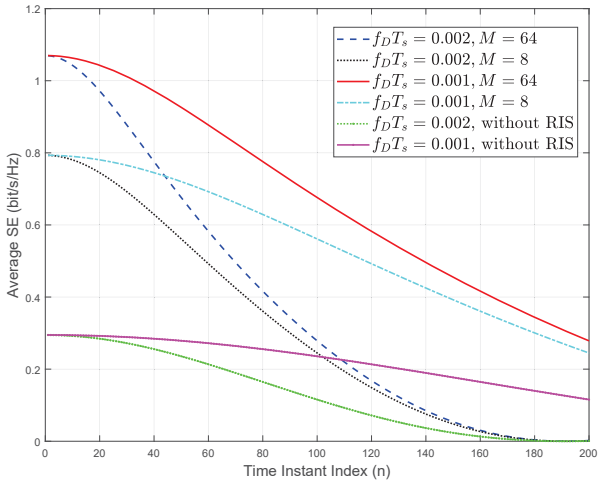

Fig. 5 – Average SE versus time instant ($N_{\mathrm{t}} = 8$)

increasing f_DT_s will accelerate the decline of the average SE. Thus, we should consider the channel aging effect when designing signal transmission time. For instance, under the condition that $f_DT_s = 0.002$, the total transmission time should be lower than 200, i.e., $\tau_c < 200$, otherwise the quality of the received signal will degrade. Furthermore, the increase of the number of RIS elements will increase the average SE. For example, compared with the traditional communication system without a RIS, at the starting time, the average SE can be improved by 181.5% when using the RIS with 8 elements, and the average SE can be improved by 263% when using the RIS with 64 elements. This shows that the use of a RIS can alleviate the channel aging effect. In addition, we can see that the change in the number of the RIS elements has no effect on the change of the time when the SE decreases 0, which is because the channel aging parameter $\rho_i[n]$ $(i \in \{0, 1\})$ is independent with the number of RIS elements *M*. Then we analyze the impact of transmission time on the system performance. Fig. 6 shows the relationship between the sum SE and the normalized Doppler shift f_DT_s under different transmission times and the number of RIS elements. When $f_DT_s = 0$, the longer the system transmission time is, the higher the sum SE of the system, which can be explained that when the uplink transmission time is fixed, the longer the total signal transmission process, the longer the proportion of downlink transmission time, and the greater the SINR of the considered system, therefore, the higher the average SE of the system. However, with the increase of the Doppler shift, the spectral efficiency of the system with longer signal transmission time decreases more sharply. This is because the increase in transmission time will lead to a more serious channel aging effect on the system. Last but not least, although the sum SE degrades with the increase of the transmission time and the normalized Doppler shift, the usage of a RIS can effectively alleviate the negative effect brought by channel aging. For example, when the normalized Doppler shift $f_DT_s = 0$ and the system transmission time $\tau_c = 100$, compared with the traditional communication system without a RIS, at the starting time, the sum SE can be improved by 77% when using the RIS with 8 elements, and the average SE can be improved by 97% when using the RIS with 64 elements.

Fig. 7 shows the sum SE under the condition of spatial correlation of RIS elements. We set the number of the antennas at the BS $N_{\mathrm{t}} = 8$, the number of RIS elements $M = 16$, the transmit power of pilot signal $P_p = 20$ dBm. We can see that compared with the system with uncorrelated channels, when we consider the channel correlation, the sum SE varies slightly differently due to the dominance of the direct channel. However, when considering the case without the direct link, the impact of spatial correlation degrades the sum SE by 13% over time instant compared with the sum SE of the system with uncorrelated cascaded links. Compared with the system with the signal transmitted from the BS to the user through

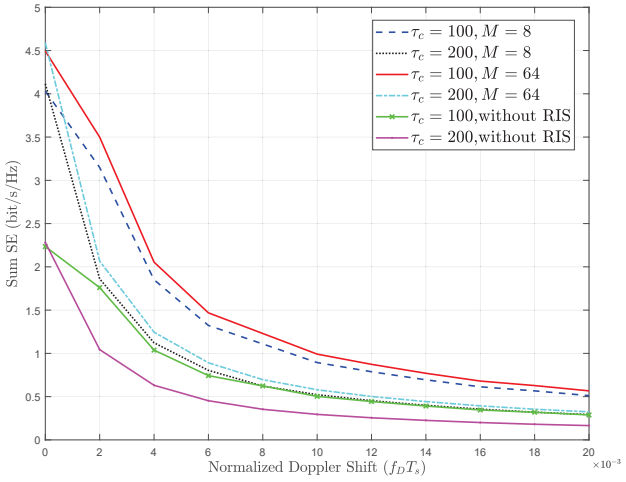

Fig. 6 – Sum SE versus normalized Doppler shift f_DT_s ($N_{\mathrm{t}} = 8$)

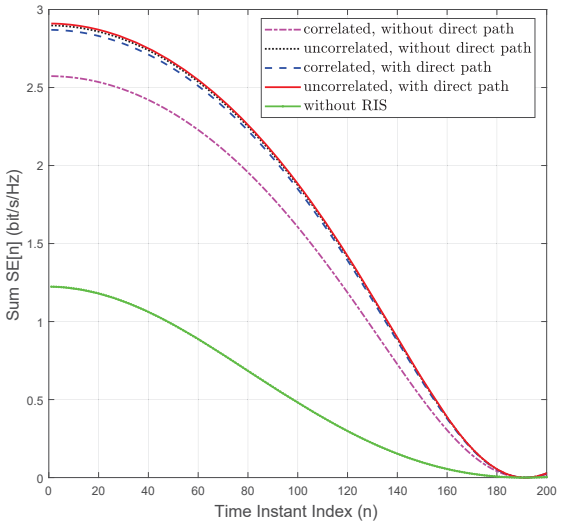

Fig. 7 – Sum SE versus time constant ($f_dT_s = 0.002$, $M = 16$)

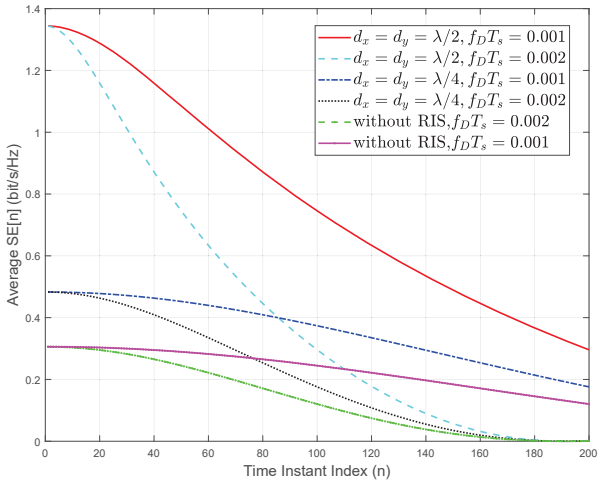

Fig. 8 – Average SE versus different size of the RIS elements and Doppler shift

an independent Rayleigh channel, the signal transmitted through a RIS correlated channel, the sum SE can be improved by 110%, which validates the efficiency of the application of the RIS in the communication system.

Fig. 8 shows the average SE under the different sizes of RIS elements and values of Doppler shift. Note that we assume that $d_{\mathrm{H}} = d_{\mathrm{V}}$. The larger the area of the elements, the higher the average SE. Furthermore, the larger the Doppler shift of the system, the faster the decline rate of the average SE. However, the change of d_{H} and d_{V} do not have an impact on the time when the average SE reaches to 0, which can be proved that $\rho_i[n]$ $(i \in \{0,1\})$ is independent of the size and the number of RIS elements. Finally, the RIS-assisted system has a higher SE compared with the traditional system without a RIS at the starting point, which proves the superiority of RISs in the wireless communication system.

5. CONCLUSION

In this paper, we analyze the performance of RIS-assisted MISO systems by considering the spatially correlated Rayleigh fading channels, the effect of channel aging, and channel estimation errors, we derive the expressions of SE of the system by employing the MRT precoding method at the BS. The results show that the use of RIS and the increase in transmit power of the pilot signal can make up for the negative effect brought about by channel aging, and the increase in the spatial correlation of RIS elements decreases the spectrum efficiency.

There are several promising directions worthy of further investigation by extending this work. For example, we only investigate the spectral efficiency, other performance metrics such as the OP and bit error rate can be analyzed. Besides, we can consider different precoding methods such as zero-forcing precoding and the MMSE precoding method.

APPENDIX

PROOF OF COROLLARY 1

We can compute each term of *(25)* as

(1) Compute $I_{0,kn}$: According to *(21)*, we have

$$\begin{aligned}\mathbb{E}\left(\boldsymbol{G}_k[n]\boldsymbol{f}_k[n]\right) &= \mathbb{E}\left(\left(\bar{\boldsymbol{G}}_k[n]+\boldsymbol{G}_{e,k}[n]\right)\boldsymbol{f}_k[n]\right)\\ &= \zeta[n]\mathbb{E}\left(\bar{\boldsymbol{G}}_k[n]\left(\bar{\boldsymbol{G}}[n]\right)^{\mathrm{H}}\right) \qquad (A1)\end{aligned}$$

which can be obtained by the fact that $\boldsymbol{G}_{\mathrm{e},k}[n]$ and $\boldsymbol{f}_{\mathrm{k}}[n]$ are independent of each other, thus $\mathbb{E}\left(\boldsymbol{G}_{\mathrm{e},k}[n]\boldsymbol{f}_{\mathrm{k}}[n]\right)=0$.

$\mathbb{E}\left(\bar{\boldsymbol{G}}_k[n]\left(\bar{\boldsymbol{G}}_k[n]\right)^{\mathrm{H}}\right)$ can be written as

$$\begin{aligned}&\mathbb{E}\left(\bar{\boldsymbol{G}}_k[n]\left(\bar{\boldsymbol{G}}_k[n]\right)^{\mathrm{H}}\right) = \rho_0^2[n]\mathbb{E}\left(\hat{\boldsymbol{G}}_{0,k}[n]\hat{\boldsymbol{G}}_{0,k}^{\mathrm{H}}[n]\right)\\ &+\rho_1^2[n]\mathbb{E}\left(\boldsymbol{v}[n]\hat{\boldsymbol{G}}_{0,k}[n]\boldsymbol{v}^{\mathrm{H}}[n]\hat{\boldsymbol{G}}_{0,k}^{\mathrm{H}}[n]\right) \qquad (A2)\end{aligned}$$

Assume $\bar{\boldsymbol{G}}_k[n] = [\bar{\boldsymbol{g}}_1[n],...,\bar{\boldsymbol{g}}_i[n],...,\bar{\boldsymbol{g}}_n[n]]$, $\bar{\boldsymbol{g}}_i[n] = [\bar{\boldsymbol{g}}_{1i}[n],...,\bar{\boldsymbol{g}}_{ki}[n],...,\bar{\boldsymbol{g}}_{Ki}[n]]^{\mathrm{T}}$ $i \in \{1,...,K\}$, $\bar{\boldsymbol{g}}_{ki}[n]$ satisfies

$$\bar{\boldsymbol{g}}_{ki}[n] = \rho_0[n]\hat{\boldsymbol{g}}_{\mathrm{d},k}^{\mathrm{H}}[n] + \rho_1[n]\boldsymbol{v}^{\mathrm{H}}[n]\hat{\boldsymbol{G}}_{0,k}^{\mathrm{H}}[n] \qquad (A3)$$

We set $\bar{\boldsymbol{g}}_{ki}[n] = \boldsymbol{c}_i[n] + \boldsymbol{d}_i[n]$, where $\boldsymbol{c}_i[n] \triangleq \rho_0[n]\hat{\boldsymbol{g}}_{\mathrm{d},k}^{\mathrm{H}}[n]$, $\boldsymbol{d}_i[n] \triangleq \rho_1[n]\boldsymbol{v}^{\mathrm{H}}[n]\hat{\boldsymbol{G}}_{0,k}^{\mathrm{H}}[n]$. For $\hat{\boldsymbol{g}}_{\mathrm{d},k}[n] \sim \mathcal{CN}\left(\boldsymbol{0}, \frac{P_p\beta_{\mathrm{d},k}^2}{\sigma_b^2+P_p\beta_{\mathrm{d},k}}\boldsymbol{I}_{\mathrm{N}_t}\right)$, thus $\boldsymbol{c}_i[n] \sim \mathcal{CN}\left(\boldsymbol{0}, \frac{\rho_0^2[n]P_p\beta_{\mathrm{d},k}^2}{\sigma_b^2+P_p\beta_{\mathrm{d},k}}\boldsymbol{I}_{\mathrm{N}_t}\right)$. For $\boldsymbol{d}_i[n]$, $\boldsymbol{v}^{\mathrm{H}}[n]\hat{\boldsymbol{G}}_{0,k}^{\mathrm{H}}[n] = \sum_{m=1}^{M}\boldsymbol{v}_m[n]\hat{\boldsymbol{g}}_{0,km}[n]$, because $\hat{\boldsymbol{g}}_{0,km}[n] \sim \mathcal{CN}\left(\boldsymbol{0}, \frac{\beta_{0,k}\hat{\sigma}_{e1,k}^2}{\hat{\sigma}_{e1,k}^2+\hat{\sigma}_{e2,k}^2+\hat{\sigma}_c^2\sigma_b^2}\boldsymbol{I}_{\mathrm{N}_t}\right)$, thus $\boldsymbol{v}^{\mathrm{H}}[n]\hat{\boldsymbol{G}}_{0,k}^{\mathrm{H}}[n] \sim \mathcal{CN}\left(\boldsymbol{0}, \frac{M\beta_{0,k}\hat{\sigma}_{e1,k}^2}{\hat{\sigma}_{e1,k}^2+\hat{\sigma}_{e2,k}^2+\hat{\sigma}_c^2\hat{\sigma}_b^2}\boldsymbol{I}_{\mathrm{N}_t}\right)$, so we can get $\boldsymbol{d}_i[n] \sim \mathcal{CN}\left(\boldsymbol{0}, \frac{M\rho_1^2[n]\beta_{0,k}\sigma_{e1,k}^2}{\sigma_{e1,k}^2+\sigma_{e2,k}^2+\sigma_b^2\sigma_c^2}\right)$. Thus we can obtain the distribution of $\bar{\boldsymbol{g}}_{ki}[n]$ as

$$\bar{\boldsymbol{g}}_{ki}[n] \sim \mathcal{CN}\left(\boldsymbol{0}, \left(\frac{\rho_0^2[n]p_p\beta_{d,k}^2}{\sigma_b^2+p_p\beta_{d,k}} + \frac{M\rho_1^2[n]\beta_{0,k}\sigma_{e1,k}^2}{\sigma_{e1,k}^2+\sigma_{e2,k}^2+\sigma_b^2\sigma_c^2}\right)\boldsymbol{I}_K\right) \qquad (A4)$$

$\bar{\boldsymbol{G}}_k[n]$ follows the complex Gaussian distribution, which is given by

$$\bar{\boldsymbol{G}}_k[n] \sim \mathcal{CN}\left(\boldsymbol{0}, \boldsymbol{I}_{\mathrm{N}_t}\otimes\left(\frac{\rho_0^2[n]p_p\beta_{\mathrm{d},k}^2}{\sigma_b^2+p_p\beta_{\mathrm{d},k}} + \frac{M\rho_1^2[n]\beta_{0,k}\sigma_{e1,k}^2}{\sigma_{e1,k}^2+\sigma_{e2,k}^2+\sigma_b^2\sigma_c^2}\right)\boldsymbol{I}_K\right) \qquad (A5)$$

$\bar{\boldsymbol{G}}_k[n]\bar{\boldsymbol{G}}_k^{\mathrm{H}}[n]$ has a complex valued central Wishart distribution [41] as

$$\bar{\boldsymbol{G}}_k[n]\bar{\boldsymbol{G}}_k^{H}[n] \sim \mathrm{W}_K\left(N_{\mathrm{t}}, \mathbf{0}, \left(\frac{\rho_0^2[n]p_p\beta_{d,k}^2}{\sigma_b^2+p_p\beta_{d,k}}+\frac{M\rho_1^2[n]\beta_{0,k}\sigma_{e1,k}^2}{\sigma_{e1,k}^2+\sigma_{e2,k}^2+\sigma_b^2\sigma_c^2}\right)\boldsymbol{I}_K\right) \quad (A6)$$

Therefore, we have

$$\mathbb{E}\left(\bar{\boldsymbol{G}}_k[n]\bar{\boldsymbol{G}}_k^{\mathrm{H}}[n]\right) = N_{\mathrm{t}}\left(\frac{\rho_0^2[n]p_p\beta_{\mathrm{d},k}^2}{\sigma_b^2+p_p\beta_{\mathrm{d},k}}+\frac{M\rho_1^2[n]\beta_{0,k}\sigma_{e1,k}^2}{\sigma_{e1,k}^2+\sigma_{e2,k}^2+\sigma_b^2\sigma_c^2}\right) \quad (A7)$$

Thus, we can obtain $I_{0,kn}$.

(2) Compute $I_{1,kn}$: According to $\mathrm{Var}(\cdot) = \mathbb{E}\left((\cdot)^2\right) - \left(\mathbb{E}(\cdot)\right)^2$, we obtain

$$\mathrm{Var}\left(\boldsymbol{G}_k[n]\boldsymbol{f}_k[n]\right) = \mathbb{E}\left(\left(\boldsymbol{G}_k[n]\boldsymbol{f}_k[n]\right)^2\right) - \left(\mathbb{E}\left(\boldsymbol{G}_k[n]\boldsymbol{f}_k[n]\right)\right)^2 \quad (A8)$$

For $\mathbb{E}\left(\left(\boldsymbol{G}_k[n]\boldsymbol{f}_k[n]\right)^2\right)$

$$\mathbb{E}\left(\left(\boldsymbol{G}_k[n]\boldsymbol{f}_k[n]\right)^2\right) = \mathbb{E}\left(\left(\left(\bar{\boldsymbol{G}}_k[n]+\boldsymbol{G}_{e,k}[n]\right)\boldsymbol{f}_k[n]\right)^2\right) = \left(\mathbb{E}\left(\bar{\boldsymbol{G}}_k[n]\boldsymbol{f}_k[n]\right)\right)^2 + \mathbb{E}\left(\boldsymbol{G}_{e,k}[n]\boldsymbol{f}_k[n]\boldsymbol{f}_k^{\mathrm{H}}[n]\boldsymbol{G}_{e,k}^{\mathrm{H}}[n]\right) \quad (A9)$$

where $\left(\mathbb{E}\left(\bar{\boldsymbol{G}}_k[n]\boldsymbol{f}_k[n]\right)\right)^2 = \left(\mathbb{E}\left(\boldsymbol{G}_k[n]\boldsymbol{f}_k[n]\right)\right)^2$, thus

$$\mathrm{Var}\left(\boldsymbol{G}_k[n]\boldsymbol{f}_k[n]\right) = \mathbb{E}\left(\boldsymbol{G}_{e,k}[n]\boldsymbol{G}_{e,k}^{\mathrm{H}}[n]\right)\mathbb{E}\left(\boldsymbol{f}_k[n]\boldsymbol{f}_k^{\mathrm{H}}[n]\right) \quad (A10)$$

For $\mathbb{E}\left(\boldsymbol{f}_k[n]\boldsymbol{f}_k^{\mathrm{H}}[n]\right)$, based on *(23)*, we obtain $\mathbb{E}\left(\boldsymbol{F}[n]\boldsymbol{F}^{\mathrm{H}}[n]\right) = \zeta^2[n]\mathbb{E}\left(\bar{\boldsymbol{G}}_k[n]\bar{\boldsymbol{G}}_k^{\mathrm{H}}[n]\right)$, i.e.,

$$\mathbb{E}\left(\boldsymbol{f}_k[n]\boldsymbol{f}_k^{\mathrm{H}}[n]\right) = \frac{\zeta^2[n]}{N_{\mathrm{t}}}\mathbb{E}\left(\bar{\boldsymbol{G}}_k[n]\bar{\boldsymbol{G}}_k^{\mathrm{H}}[n]\right) = \zeta^2[n]\left(\frac{\rho_0^2[n]P_p\beta_{\mathrm{d},k}^2}{\sigma_b^2+P_p\beta_{\mathrm{d},k}}+\frac{M\rho_1^2[n]\beta_{0,k}\sigma_{e1,k}^2}{\sigma_{e1,k}^2+\sigma_{e2,k}^2+\sigma_b^2\sigma_c^2}\right) \quad (A11)$$

$\mathbb{E}\left(\boldsymbol{G}_{e,k}[n]\boldsymbol{G}_{e,k}^{\mathrm{H}}[n]\right)$ can be written as

$$\begin{aligned}&\mathbb{E}\left(\boldsymbol{G}_{e,k}[n]\boldsymbol{G}_{e,k}^{\mathrm{H}}[n]\right)\\ &= \mathbb{E}\left(\left(\tilde{\boldsymbol{e}}_{\mathrm{d},k}^{\mathrm{H}}[n]+\boldsymbol{v}^{\mathrm{H}}[n]\tilde{\boldsymbol{E}}_{0,k}^{\mathrm{H}}[n]\right)\left(\tilde{\boldsymbol{e}}_{\mathrm{d},k}^{\mathrm{H}}[n]+\boldsymbol{v}^{\mathrm{H}}[n]\tilde{\boldsymbol{E}}_{0,k}^{\mathrm{H}}[n]\right)^{\mathrm{H}}\right)\\ &= \mathbb{E}\left(\tilde{\boldsymbol{e}}_{\mathrm{d},k}^{\mathrm{H}}[n]\tilde{\boldsymbol{e}}_{\mathrm{d},k}[n]+\boldsymbol{v}^{\mathrm{H}}[n]\tilde{\boldsymbol{E}}_{0,k}^{\mathrm{H}}[n]\tilde{\boldsymbol{E}}_{0,k}[n]\boldsymbol{v}[n]\right)\\ &= \mathbb{E}\left(\tilde{\boldsymbol{e}}_{\mathrm{d},k}^{\mathrm{H}}[n]\tilde{\boldsymbol{e}}_{\mathrm{d},k}[n]\right)+\mathbb{E}\left(\boldsymbol{v}^{\mathrm{H}}[n]\tilde{\boldsymbol{E}}_{0,k}^{\mathrm{H}}[n]\tilde{\boldsymbol{E}}_{0,k}[n]\boldsymbol{v}[n]\right)\end{aligned} \quad (A12)$$

For $\tilde{\boldsymbol{e}}_{d,k}[n] \sim \mathcal{CN}\left(\mathbf{0}, \left(\beta_{d,k}-\frac{\rho_0^2[n]P_p\beta_{d,k}^2}{\sigma_b^2+P_p\beta_{d,k}}\right)\boldsymbol{I}_{N_t}\right)$, we can get $\mathbb{E}\left(\tilde{\boldsymbol{e}}_{\mathrm{d},k}^{\mathrm{H}}[n]\tilde{\boldsymbol{e}}_{\mathrm{d},k}[n]\right) = N_{\mathrm{t}}(\beta_{\mathrm{d},k}-\frac{\rho_0^2[n]P_p\beta_{\mathrm{d},k}^2}{\sigma_b^2+P_p\beta_{\mathrm{d},k}})$.

$\mathbb{E}\left(\boldsymbol{v}^{\mathrm{H}}[n]\tilde{\boldsymbol{E}}_{0,k}^{\mathrm{H}}[n]\tilde{\boldsymbol{E}}_{0,k}[n]\boldsymbol{v}[n]\right)$ can be written as

$$\mathbb{E}\left(\boldsymbol{v}^{\mathrm{H}}[n]\tilde{\boldsymbol{E}}_{0,k}^{\mathrm{H}}[n]\tilde{\boldsymbol{E}}_{0,k}[n]\boldsymbol{v}[n]\right) = \mathbb{E}\left(\sum_{m=1}^{M}\sum_{l=1}^{M}\exp\left(j\theta_m[n]-j\theta_l[n]\right)\tilde{\boldsymbol{e}}_{0,k}^{\mathrm{H}}[n]\tilde{\boldsymbol{e}}_{0,k}[n]\right) \quad (A13)$$

For $\tilde{\boldsymbol{e}}_{0,km}[n] \sim \mathcal{CN}\left(\mathbf{0}, \left(\beta_{0,k}-\frac{\rho_1^2[n]\beta_{0,k}\sigma_{e1,k}^2}{\sigma_{e1,k}^2+\sigma_{e2,k}^2+\sigma_c^2\sigma_b^2}\right)\boldsymbol{I}_{N_t}\right)$, we can get $\mathbb{E}\left(\tilde{\boldsymbol{e}}_{0,k}^{H}[n]\tilde{\boldsymbol{e}}_{0,k}[n]\right) = N_t\left(\beta_{0,k}-\frac{\rho_1^2[n]\beta_{0,k}\sigma_{e1,k}^2}{\sigma_{e1,k}^2+\sigma_{e2,k}^2+\sigma_c^2\sigma_b^2}\right)$, thus

$$\mathbb{E}\left(\boldsymbol{v}^{\mathrm{H}}[n]\tilde{\boldsymbol{E}}_{0,k}^{\mathrm{H}}[n]\tilde{\boldsymbol{E}}_{0,k}[n]\boldsymbol{v}[n]\right) = MN_{\mathrm{t}}\left(\beta_{0,k}-\frac{\rho_1^2[n]\beta_{0,k}\sigma_{e1,k}^2}{\sigma_{e1,k}^2+\sigma_{e2,k}^2+\sigma_c^2\sigma_b^2}\right) \quad (A14)$$

$$\mathbb{E}\left(\boldsymbol{G}_{e,k}[n]\boldsymbol{G}_{e,k}^{\mathrm{H}}[n]\right) = N_{\mathrm{t}}\left(\beta_{d,k}-\frac{\rho_0^2[n]P_p\beta_{d,k}^2}{\sigma_b^2+P_p\beta_{d,k}}\right) + MN_{\mathrm{t}}\left(\beta_{0,k}-\frac{\rho_1^2[n]\beta_{0,k}\sigma_{e1,k}^2}{\sigma_{e1,k}^2+\sigma_{e2,k}^2+\sigma_c^2\sigma_b^2}\right) \quad (A15)$$

Thus, we obtain

$$\mathrm{Var}\left(\boldsymbol{G}_k[n]\boldsymbol{f}_k[n]\right) = \left(\left(\beta_{\mathrm{d},k}-\frac{\rho_0^2[n]P_p\beta_{\mathrm{d},k}^2}{\sigma_b^2+P_p\beta_{\mathrm{d},k}}\right)+M\left(\beta_{0,k}-\frac{\rho_1^2[n]\beta_{0,k}\sigma_{e1,k}^2}{\sigma_{e1,k}^2+\sigma_{e2,k}^2+\sigma_c^2\sigma_b^2}\right)\right)\times\zeta^2[n]N_{\mathrm{t}}\left(\frac{\rho_0^2[n]P_p\beta_{\mathrm{d},k}^2}{\sigma_b^2+P_p\beta_{\mathrm{d},k}}+\frac{M\rho_1^2[n]\beta_{0,k}\sigma_{e1,k}^2}{\sigma_{e1,k}^2+\sigma_{e2,k}^2+\sigma_c^2\sigma_b^2}\right) \quad (A16)$$

(3) Compute $I_{2,kn}$: Following the same approach as for the derivation of *(29)*, we obtain *(30)* to complete the proof.

(4) Compute $I_{3,kn}$: We can easily prove that $E\left(|\omega_k[n]|^2\right) = \sigma_k^2$.

ACKNOWLEDGEMENT

This work was supported by Natural Science Foundation of Jiangsu Province, Major Project under Grant BK20212002.

REFERENCES

[1] Jiayi Zhang, Emil Björnson, Michail Matthaiou, Derrick Wing Kwan Ng, Hong Yang, and David J. Love. "Prospective Multiple Antenna Technologies for Beyond 5G". In: *IEEE Journal on Selected Areas in Communications* 38.8 (2020), pp. 1637–1660. DOI: 10.1109/JSAC.2020.3000826.

[2] Abla Kammoun, Mérouane Debbah, Mohamed-Slim Alouini, et al. "Asymptotic analysis of RZF over double scattering channels with MMSE estimation". In: *IEEE Transactions on Wireless Communications* 18.5 (2019), pp. 2509–2526.

[3] Chongwen Huang, Ronghong Mo, and Chau Yuen. "Reconfigurable Intelligent Surface Assisted Multiuser MISO Systems Exploiting Deep Reinforcement Learning". In: *IEEE Journal on Selected Areas in Communications* 38.8 (2020), pp. 1839–1850. DOI: 10.1109/JSAC.2020.3000835.

[4] Marco Di Renzo, Merouane Debbah, Dinh-Thuy Phan-Huy, Alessio Zappone, Mohamed-Slim Alouini, Chau Yuen, Vincenzo Sciancalepore, George C Alexandropoulos, Jakob Hoydis, Haris Gacanin, et al. "Smart radio environments empowered by reconfigurable AI meta-surfaces: An idea whose time has come". In: *EURASIP Journal on Wireless Communications and Networking* 2019.1 (2019), pp. 1–20.

[5] Yajun Zhao, Jiayi Zhang, and Bo Ai. "Applications of Reconfigurable Intelligent Surface in Smart High Speed Train Communications". In: *ZTE Commun.* 27.4 (Aug. 2021), pp. 36–43.

[6] Enyu Shi, Jiayi Zhang, Shuaifei Chen, Jiakang Zheng, Yan Zhang, Derrick Wing Kwan Ng, and Bo Ai. "Wireless Energy Transfer in RIS-Aided Cell-Free Massive MIMO Systems: Opportunities and Challenges". In: *IEEE Communications Magazine* 60.3 (2022), pp. 26–32. DOI: 10.1109/MCOM.001.2100671.

[7] Ertugrul Basar, Marco Di Renzo, Julien De Rosny, Merouane Debbah, Mohamed-Slim Alouini, and Rui Zhang. "Wireless Communications Through Reconfigurable Intelligent Surfaces". In: *IEEE Access* 7 (2019), pp. 116753–116773. DOI: 10.1109/ACCESS.2019.2935192.

[8] Jiayi Zhang, Heng Liu, Qingqing Wu, Yu Jin, Yuanbin Chen, Bo Ai, Shi Jin, and Tie Jun Cui. "RIS-Aided Next-Generation High-Speed Train Communications: Challenges, Solutions, and Future Directions". In: *IEEE Wireless Communications* 28.6 (2021), pp. 145–151. DOI: 10.1109/MWC.001.2100170.

[9] Hongyang Du, Jiawen Kang, Dusit Niyato, Jiayi Zhang, and Dong In Kim. "Reconfigurable Intelligent Surface-Aided Joint Radar and Covert Communications: Fundamentals, Optimization, and Challenges". In: *IEEE Vehicular Technology Magazine* 17.3 (2022), pp. 54–64. DOI: 10.1109/MVT.2022.3169292.

[10] Yuanbin Chen, Ying Wang, Jiayi Zhang, Ping Zhang, and Lajos Hanzo. "Reconfigurable Intelligent Surface (RIS)-Aided Vehicular Networks: Their Protocols, Resource Allocation, and Performance". In: *IEEE Vehicular Technology Magazine* 17.2 (2022), pp. 26–36.

[11] Yifei Yang, Beixiong Zheng, Shuowen Zhang, and Rui Zhang. "Intelligent reflecting surface meets OFDM: Protocol design and rate maximization". In: *IEEE Transactions on Communications* 68.7 (2020), pp. 4522–4535.

[12] Bayan Al-Nahhas, Anas Chaaban, et al. "Intelligent reflecting surface assisted MISO downlink: Channel estimation and asymptotic analysis". In: *GLOBECOM 2020-2020 IEEE Global Communications Conference*. IEEE. 2020, pp. 1–6.

[13] Hibatallah Alwazani, Abla Kammoun, Anas Chaaban, Mérouane Debbah, Mohamed-Slim Alouini, et al. "Intelligent reflecting surface-assisted multi-user MISO communication: Channel estimation and beamforming design". In: *IEEE Open Journal of the Communications Society* 1 (2020), pp. 661–680.

[14] Anas M Salhab and Monjed H Samuh. "Accurate performance analysis of reconfigurable intelligent surfaces over Rician fading channels". In: *IEEE Wireless Communications Letters* 10.5 (2021), pp. 1051–1055.

[15] Dhanushka Kudathanthirige, Dulaj Gunasinghe, and Gayan Amarasuriya. "Performance analysis of intelligent reflective surfaces for wireless communication". In: *ICC 2020-2020 IEEE International Conference on Communications (ICC)*. IEEE. 2020, pp. 1–6.

[16] Anastasios K Papazafeiropoulos. "Impact of general channel aging conditions on the downlink performance of massive MIMO". In: *IEEE Transactions on Vehicular Technology* 66.2 (2016), pp. 1428–1442.

[17] Kien T Truong and Robert W Heath. "Effects of channel aging in massive MIMO systems". In: *Journal of Communications and Networks* 15.4 (2013), pp. 338–351.

[18] Olga Boric-Lubecke, Victor M. Lubecke, Amy D. Droitcour, Byung-Kwon Park, and Aditya Singh. "Physiological Doppler Radar Overview". In: *Doppler Radar Physiological Sensing*. 2016, pp. 69–94. DOI: 10.1002/9781119078418.ch4.

[19] Jiakang Zheng, Jiayi Zhang, Emil Björnson, and Bo Ai. "Impact of Channel Aging on Cell-Free Massive MIMO Over Spatially Correlated Channels". In: *IEEE Transactions on Wireless Communications* 20.10 (2021), pp. 6451–6466. DOI: 10.1109/TWC.2021.3074421.

[20] Ribhu Chopra, Chandra R. Murthy, Himal A. Suraweera, and Erik G. Larsson. "Performance Analysis of FDD Massive MIMO Systems Under Channel Aging". In: *IEEE Transactions on Wireless Communications* 17.2 (2018), pp. 1094–1108. DOI: 10.1109/TWC.2017.2775629.

[21] Emil Björnson and Luca Sanguinetti. "Rayleigh fading modeling and channel hardening for reconfigurable intelligent surfaces". In: *IEEE Wireless Communications Letters* 10.4 (2020), pp. 830–834.

[22] Neel Kanth Kundu and Matthew R. McKay. "Channel Estimation for Reconfigurable Intelligent Surface Aided MISO Communications: From LMMSE to Deep Learning Solutions". In: *IEEE Open Journal of the Communications Society* 2 (2021), pp. 471–487. DOI: 10.1109/OJCOMS.2021.3063171.

[23] Yan Zhang, Jiayi Zhang, Derrick Wing Kwan Ng, Huahua Xiao, and Bo Ai. "Performance analysis of reconfigurable intelligent surface assisted systems under channel aging". In: *Intelligent and Converged Networks* 3.1 (2022), pp. 74–85. DOI: 10.23919/ICN.2022.0002.

[24] Ming-Min Zhao, Qingqing Wu, Min-Jian Zhao, and Rui Zhang. "Intelligent Reflecting Surface Enhanced Wireless Networks: Two-Timescale Beamforming Optimization". In: *IEEE Transactions on Wireless Communications* 20.1 (2021), pp. 2–17. DOI: 10.1109/TWC.2020.3022297.

[25] A. Burg, S. Haene, D. Perels, P. Luethi, N. Felber, and W. Fichtner. "Algorithm and VLSI architecture for linear MMSE detection in MIMO-OFDM systems". In: *2006 IEEE International Symposium on Circuits and Systems*. 2006, 4 pp.-. DOI: 10.1109/ISCAS.2006.1693531.

[26] Duy HN Nguyen and Tho Le-Ngoc. "MMSE precoding for multiuser MISO downlink transmission with non-homogeneous user SNR conditions". In: *EURASIP Journal on Advances in Signal Processing* 2014.1 (2014), pp. 1–12.

[27] Shahram Zarei, Wolfgang Gerstacker, and Robert Schober. "Low-complexity widely-linear precoding for downlink large-scale MU-MISO systems". In: *IEEE Communications Letters* 19.4 (2015), pp. 665–668.

[28] Qurrat-Ul-Ain Nadeem, Hibatallah Alwazani, Abla Kammoun, Anas Chaaban, Mérouane Debbah, and Mohamed-Slim Alouini. "Intelligent Reflecting Surface-Assisted Multi-User MISO Communication: Channel Estimation and Beamforming Design". In: *IEEE Open Journal of the Communications Society* 1 (2020), pp. 661–680. DOI: 10.1109/OJCOMS.2020.2992791.

[29] Jie Huang, Cheng-Xiang Wang, Yingzhuo Sun, Rui Feng, Jialing Huang, Bolun Guo, Zhimeng Zhong, and Tie Jun Cui. "Reconfigurable Intelligent Surfaces: Channel Characterization and Modeling". In: *Proceedings of the IEEE* 110.9 (2022), pp. 1290–1311. DOI: 10.1109/JPROC.2022.3186087.

[30] Alexandros–Apostolos A Boulogeorgos and Angeliki Alexiou. "How much do hardware imperfections affect the performance of reconfigurable intelligent surface-assisted systems?" In: *IEEE Open Journal of the Communications Society* 1 (2020), pp. 1185–1195.

[31] Xuewen Qian, Marco Di Renzo, Jiang Liu, Abla Kammoun, and M-S Alouini. "Beamforming through reconfigurable intelligent surfaces in single-user MIMO systems: SNR distribution and scaling laws in the presence of channel fading and phase noise". In: *IEEE Wireless Communications Letters* 10.1 (2020), pp. 77–81.

[32] Ribhu Chopra, Chandra R Murthy, Himal A Suraweera, and Erik G Larsson. "Performance analysis of FDD massive MIMO systems under channel aging". In: *IEEE Transactions on Wireless Communications* 17.2 (2017), pp. 1094–1108.

[33] Yajing Guo, Jiayi Zhang, Zhaohua Lu, and Minghui Wang. "Beam Tracking and Coverage Enhancement Algorithm for Mobile Users with Intelligent Reflecting Surface". In: *ZTE Commun.* 27.2 (Apr. 2021), pp. 54–59.

[34] Marco Di Renzo, Alessio Zappone, Merouane Debbah, Mohamed-Slim Alouini, Chau Yuen, Julien De Rosny, and Sergei Tretyakov. "Smart radio environments empowered by reconfigurable intelligent surfaces: How it works, state of research, and the road ahead". In: *IEEE Journal on Selected Areas in Communications* 38.11 (2020), pp. 2450–2525.

[35] Heng Liu, Jiayi Zhang, Qingqing Wu, Huahua Xiao, and Bo Ai. "ADMM based channel estimation for RISs aided millimeter wave communications". In: *IEEE communications letters* 25.9 (2021), pp. 2894–2898.

[36] Yu Jin, Jiayi Zhang, Xiaodan Zhang, Huahua Xiao, Bo Ai, and Derrick Wing Kwan Ng. "Channel estimation for semi-passive reconfigurable intelligent surfaces with enhanced deep residual networks". In: *IEEE transactions on vehicular technology* 70.10 (2021), pp. 11083–11088.

[37] Yan Zhang, Jiayi Zhang, Marco Di Renzo, Huahua Xiao, and Bo Ai. "Reconfigurable intelligent surfaces with outdated channel state Information: Centralized vs. distributed deployments". In: *IEEE Transactions on Communications* 70.4 (2022), pp. 2742–2756.

[38] William C Jakes. *Mobile microwave communication*. 1974.

[39] Jiakang Zheng, Jiayi Zhang, Emil Björnson, and Bo Ai. "Impact of channel aging on cell-free massive MIMO over spatially correlated channels". In: *IEEE Transactions on Wireless Communications* 20.10 (2021), pp. 6451–6466.

[40] Wankai Tang, Ming Zheng Chen, Xiangyu Chen, Jun Yan Dai, Yu Han, Marco Di Renzo, Yong Zeng, Shi Jin, Qiang Cheng, and Tie Jun Cui. "Wireless communications with reconfigurable intelligent surface: Path loss modeling and experimental measurement". In: *IEEE Transactions on Wireless Communications* 20.1 (2020), pp. 421–439.

[41] Robb J Muirhead. *Aspects of multivariate statistical theory*. John Wiley & Sons, 2009.

AUTHORS

Yu Lu is currently working towards a master's degree in communication engineering from Beijing Jiaotong University, Beijing, China. Her research interests include reconfigurable intelligent surfaces and its performance analysis.

Yan Zhang is currently working towards a master's degree in communication engineering from Beijing Jiaotong University, Beijing, China. Her research interests include reconfigurable intelligent surfaces and performance analysis of wireless communications over generalized fading channels.

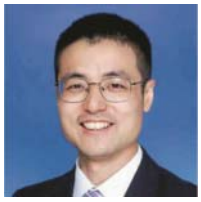

Jiayi Zhang received BSc and PhD degrees in communication engineering from Beijing Jiaotong University, China in 2007 and 2014, respectively. Since 2016 he has been a professor with the School of Electronic and Information Engineering, Beijing Jiaotong University, China. From 2014 to 2016 he was a postdoctoral research associate with the Department of Electronic Engineering, Tsinghua University, China. From 2014 to 2015, he was also a Humboldt Research Fellow in the Institute for Digital Communications, Friedrich-Alexander-University Erlangen-Nürnberg (FAU), Germany. From 2012 to 2013, he was a visiting scholar at the Wireless Group, University of Southampton, United Kingdom. His current research interests include cell-free massive MIMO, reconfigurable intelligent surface (RIS), communication theory and applied mathematics. Dr. Zhang received the Best Paper Awards at the WCSP 2017 and IEEE APCC 2017, the URSI Young Scientist Award in 2020, and the IEEE ComSoc Asia-Pacific Outstanding Young Researcher Award in 2020. He was recognized as an exemplary reviewer of the IEEE Communications letters in 2015-2017. He was also recognized as an exemplary reviewer of the IEEE Transactions on communications in 2017-2019. He was the lead guest editor of the special issue on "Multiple Antenna Technologies for Beyond 5G" of the IEEE Journal on selected areas in communications. He currently serves as an associate editor for IEEE Transactions on communications, IEEE communications letters, IEEE Access and IET communications.

Bo Ai received his master's degree and PhD degrees from Xidian University in China. He graduated from Tsinghua University with the honor of Excellent Postdoctoral Research Fellow at Tsinghua University in 2007. He was a visiting professor at EE Department, Stanford University in 2015. He is now working at Beijing Jiaotong University as a full professor and Ph. D. candidate advisor. He is the Deputy Director of State Key Lab of Rail Traffic Control and Safety, and the Deputy Director of International Joint Research Center. He is one of the main responsible people for Beijing "Urban rail operation control system" International Science and Technology Cooperation Base, and the backbone member of the Innovative Engineering Based jointly granted by Chinese Ministry of Education and the State Administration of Foreign Experts Affairs.He has authored/co-authored eight books and published over 300 academic research papers in his research area. He holds 26 invention patents. He has been the research team leader for 26 national projects and has won some important scientific research prizes. Five papers have been the ESI highly-cited paper. He has been notified by Council of Canadian Academies (CCA) that, based on Scopus database, Prof. Bo Ai has been listed as one of the Top 1% authors in his field all over the world. Prof. Bo Ai has also been feature interviewed by IET Electronics Letters. His interests include the research and applications of channel measurement and channel modeling, dedicated mobile communications for rail traffic systems. Prof. Bo Ai is a fellow of the Institution of Engineering and Technology (IET Fellow), and IEEE VTS distinguished lecturer. He is an IEEE VTS Beijing Chapter vice chair. IEEE BTS Xi'an Chapter chair. He was as a co-chair or a session/track chair for many international conferences. He is an associate editor of IEEE Antennas and Wireless Propagation Letters, IEEE Transactions on Consumer Electronics and an editorial committee member of the Wireless Personal Communications journal. He is the lead guest editor for special issues on IEEE Transactions on Vehicular Technology, IEEE Antennas and Propagations Letters, International Journal on Antennas and Propagations. He has received many awards such as Distinguished Youth Foundation and Excellent Youth Foundation from National Natural Science Foundation of China, the Qiushi Outstanding Youth Award by Hong Kong Qiushi Foundation, the New Century Talents by the Chinese Ministry of Education, the Zhan Tianyou Railway Science and Technology Award by the Chinese Ministry of Railways, and the Science and Technology New Star by the Beijing Municipal Science and Technology Commission.